# In Situ Focused Ion Beam Scanning Electron Microscope Study of Microstructural Evolution of Single Tin Particle Anode for Li-Ion Batteries

Xinwei Zhou[1, 2], Tianyi Li[1], Yi Cui[1], Yongzhu Fu[3], Yuzi Liu[2*], and Likun Zhu[1*]

[1]Department of Mechanical and Energy Engineering, Indiana University Purdue University Indianapolis, Indianapolis, IN 46202

[2]Center for Nanoscale Materials, Argonne National Laboratory, 9700 South Cass Avenue, Argonne, Illinois 60439

[3]College of Chemistry and Molecular Engineering, Zhengzhou University, Zhengzhou, Henan 450001, China

*Corresponding author: likzhu@iupui.edu (L. Zhu), yuziliu@anl.gov (Y. Liu)

This is the author's manuscript of the article published in final edited form as:

Zhou, X., Li, T., Cui, Y., Fu, Y., Liu, Y., & Zhu, L. (2019). In Situ Focused Ion Beam Scanning Electron Microscope Study of Microstructural Evolution of Single Tin Particle Anode for Li-Ion Batteries. ACS Applied Materials & Interfaces. https://doi.org/10.1021/acsami.8b13981

**Abstract**

Tin (Sn) is a potential anode material for high energy density Li-ion batteries due to its high capacity, safety, abundance and low cost. However, Sn suffers from large volume change during cycling, leading to fast degradation of the electrode. For the first time, the microstructural evolution of micrometer-sized single Sn particle was monitored by focused-ion beam (FIB) polishing and scanning electron microscopy (SEM) imaging during electrochemical cycling by in situ FIB-SEM. Our results show the formation and evolution of cracks during lithiation, evolution of porous structure during delithiation and volume expansion/contraction during cycling. The electrochemical performance and the microstructural evolution of the Sn micro-particle during cycling are directly correlated, which provides insights for understanding Sn-based electrode materials.

Keywords: Li-ion battery, single tin particle battery, in situ, focused-ion beam-scanning electron microscopy, microstructural evolution

Tin (Sn) has been considered a promising anode material for lithium-ion (Li-ion) batteries because it is non-toxic, abundant, and inexpensive and it has a theoretical specific capacity of 994 mAh $g^{-1}$.[1] However, Sn electrode has large volume change during lithiation and delithiation, which causes pulverization of active material, leading to fast capacity fading.[2-4] In order to address this issue, it is necessary to understand the microstructure evolution and electrochemical performance of Sn electrodes during cycling. In recent years, several advanced techniques have been developed to investigate the microstructural evolution of anode materials during cycling in in situ and in operando cell setups, such as transmission X-ray microscopy (TXM) [5-9] and transmission electron microscopy (TEM).[10-13] By using synchrotron TXM, either 2D projection images or 3D microstructures have been obtained to reveal the microstructure change of Sn particles during cycling.[5, 8-9, 14] However, the Sn electrodes used in these in situ studies were composed of Sn particles with different size and shapes. It is challenging to correlate the microstructural evolution of single Sn particle with the electrochemical performance of the whole cell on the multiple-particle scale. Since its first application for battery research in 2010,[15] in situ TEM has made significant contribution to reveal the microstructural evolution and phase change of electrode materials.[10-13] Although in situ TEM allows real time microstructure investigation at atomic scale resolution, the in situ cell rarely shows electrochemical performance of electrodes mainly due to the size of the samples and the corresponding ultralow capacity. To correlate the microstructural evolution and the electrochemical performance, micrometer-sized particles have to be used, which is too big for the TEM analysis and too small for X-ray characterizations in many cases. But it is appropriate for scanning electron microscopy (SEM) imaging. Recently, in situ and in operando SEM have been used to obtain the dynamic morphology change of battery materials.[16-18] Miller et. al developed an approach to carry out in situ SEM of single Li-ion battery cathode particles during electrochemical cycling using a

focused-ion beam-scanning electron microscope (FIB-SEM).[18] In this study, we adopted and optimized the approach to build a single Sn particle battery in the chamber of FIB-SEM. The microstructural evolution of a single Sn micrometer-sized particle was monitored by SEM and coupled with electrochemical characterizations.

The experiment was performed on a Zeiss Nvision 40 FIB-SEM at the Center for Nanoscale Materials, Argonne National Laboratory. The schematic of experiment setup is shown in Figure 1a. Figures 1b and c show the SEM images of the single Sn particle battery inside the FIB-SEM chamber. To build the single particle battery cell, a Sn particle (Sigma-Aldrich) was attached to the tungsten probe by ion beam carbon deposition as positive electrode. The Li metal was placed on top of the SEM stub as negative electrode. One drop of ionic liquid electrolyte (ILE) was placed on top of Li metal. The ILE was made by dissolving the Li salt, lithium bis (trifluoromethylsulfonyl) imide (LiTFSI) (Sigma-Aldrich), in a solvent of 1-butyl-1-methylpyrrolidinium bis (trifluoromethylsulfonyl) imide ($P_{14}$TFSI) (Sigma-Aldrich).[12, 19] The vapor pressure of $P_{14}$TFSI is close to zero, which makes the liquid suitable for the vacuum environment in FIB-SEM.[20] The single particle battery cycling was controlled by a Keithley 6430 sub-femtoamp remote soursemeter from Tektronix. The particle was immersed in the ILE drop during cycling and lifted out for imaging at different states of charge and discharge. In order to visualize the microstructure change of the particle, the imaging area was polished by FIB to remove ILE on the surface. The electron beam and ion beam remain closed other than taking images. Galvanostatic mode was used in all electrochemical cycling. The voltage window was between 0.01-1.2 V. The particle with a limited discharge capacity was also tested to study the microstructure change along with cycles of the materials.

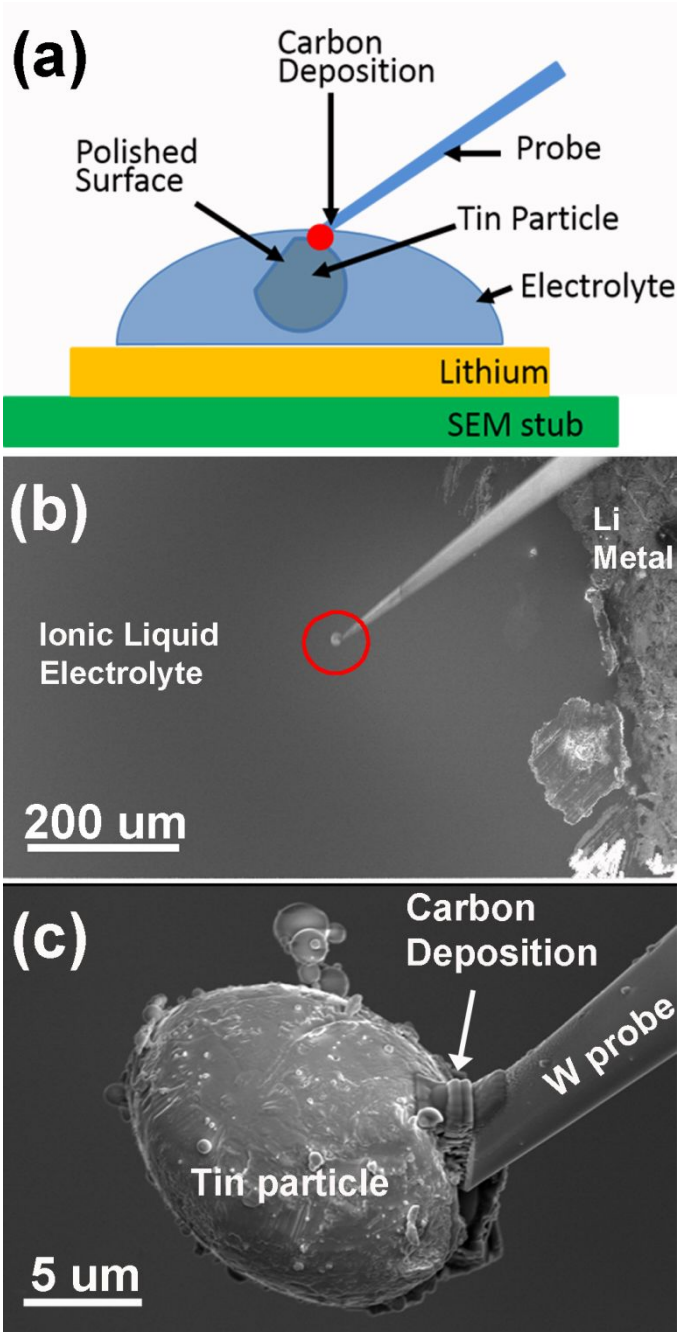


Figure 1. a) Schematic of a single Sn particle battery. b) SEM image of a single Sn particle battery showing the ILE and both Li and Sn electrodes. c) SEM image of a Sn particle attached to a tungsten probe.

As shown in Figure 2, a spherical Sn particle with 10 μm diameter was selected for the experiment. The discharging and charging current was set at 0.3 nA (about C/15 rate). The voltage profile of the

first cycle and the estimated relative volume at different states of charge are shown in Figure 2a. Figures 2b-k are SEM micrographs corresponding to the time points b-k in Figure 2a respectively. At these points, the galvanostatic discharging or charging was stopped, the particle was lifted out of ILE and polished by FIB, and then SEM images were taken on the polished surface. The voltage profile shows that the FIB polishing had a small impact on the cycling performance. After each polishing, the voltage curve was disturbed a little but quickly returned to the normal level. The voltage profile does not show the typical three plateaus as reported in the literatures, instead it shows a long plateau at 0.4 V. In order to understand this phenomenon, we have to eliminate the possible impact of FIB polishing and imaging on the voltage profile. A Sn particle was cycled at 0.15 nA without FIB polishing and imaging and the voltage profile also shows a long plateau in the lithiation process (Figure S1a). This long plateau in the first lithiation process has been observed in Sn film electrodes [21-23] and it was considered as the result of disorder in the initially formed material. [21] However, the voltage profile of Sn electrode made of the same Sn particles shows three plateaus in the first lithiation process (Figure S1b). It means that the long plateau in the first lithiation is not due to the disorder in the initially formed material. We believe that this phenomenon could be due to the large difference in Li diffusivity between Li-poor phases and Li-rich phases. As shown in Ref [24], the diffusivity of Li in Li-poor phases (before LiSn) is about one order lower than that in Li-rich phases. Due to the high diffusivity in Li-rich phases and low diffusivity in Li-poor phases (the first and the second plateaus), it is favorable to form Li-rich phases (the third plateau). As shown in Ref[25-26], when the size of Sn particles is larger and the current density is higher, the single plateau appears in the first lithiation. They have attributed this phenomenon to the slow diffusion rates of Li in Li-poor phases. As shown in Ref[21-23], the plateaus appear in the second lithiation. We believe it is due to two reasons. The first reason is the significant surface area increase due to the pulverization, which results in low current

density on the Sn surface. The second reason is the inhomogeneity of the pulverized Sn material.

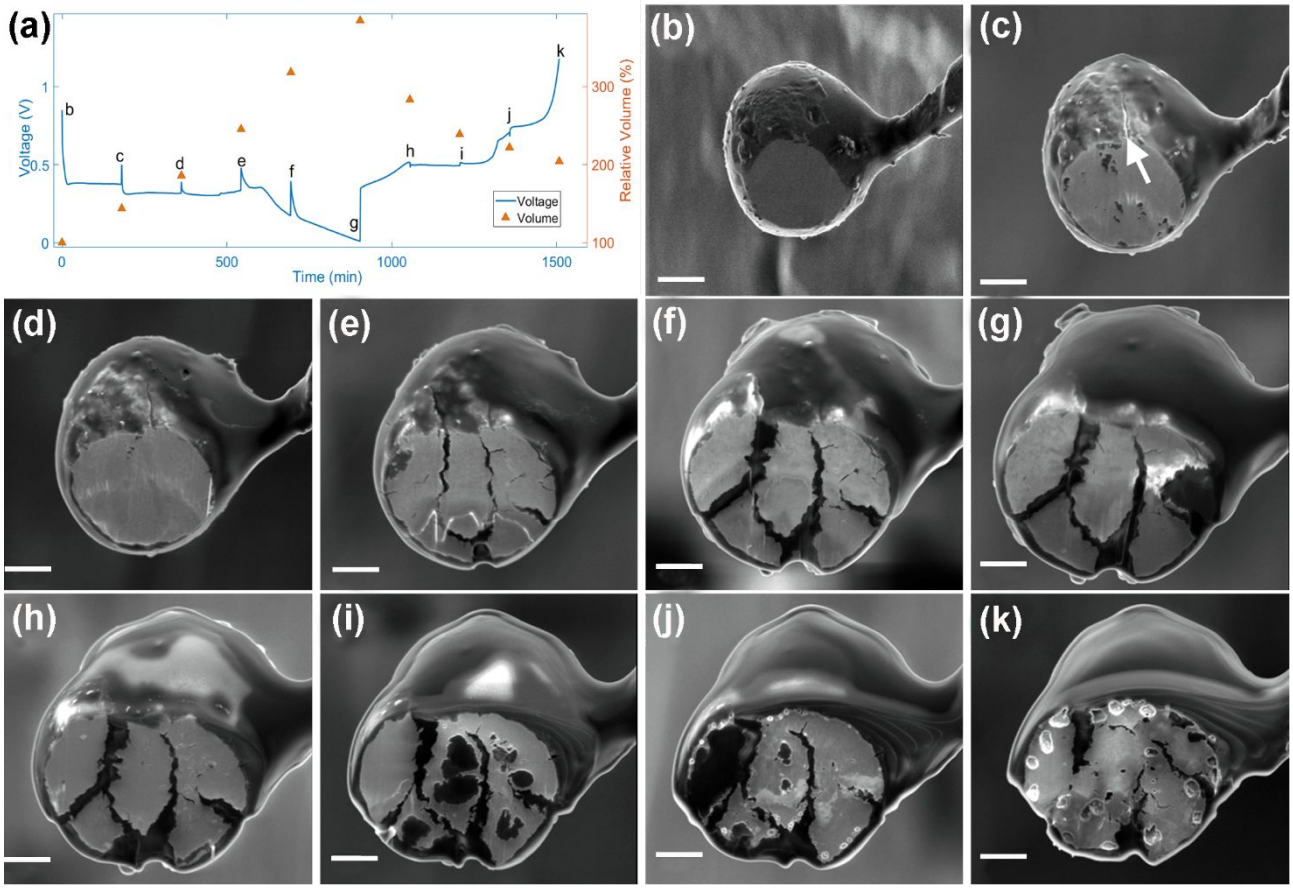


Figure 2. A Sn particle fully discharged/charged at 0.3 nA. a) Voltage profile and relative volume of the first cycle. b) SEM image of as-prepared Tin particle. c-g) SEM images of the same particle at 20%, 40%, 60%, 77% and 100% of discharge states respectively. h-k) SEM images at 25%, 50%, 75% and 100% of charge states respectively. Scale bar is 3 μm.

The relative volume in Figure 2a is estimated by images taken in FIB mode shown in Figure S2. Figure 2b shows the SEM image of particle before cycling. Figures 2c – g show the SEM images at 20%, 40%, 60%, 77% and 100% of lithiation process and the relative volumes are 144%, 186%, 246%, 318%, and 384%, respectively. These images show an increased degree of cracking of the

particle. In Figure 2c, the volume of the particle increased to 144% and a small crack appeared above the polished surface as indicated by the arrow. On the polished surface, a few concave areas appeared. In Figure 2d, these concave areas are removed during polishing, which means they are not deep cracks. In the same image, we can see that small cracks start to appear on the surface. In Figures 2e-g, the cracks keep growing and propagate into the particle. In Figure 2g, a dark area appears on the right side of the particle. We believe that it is not a big crack and it is a big concave area due to the expansion of the material. The volume expansion of particle is almost homogeneous in the first 60% of lithiation (Figures 2c, d and e). When the cracks become larger (Figures 2f and g), the expansion is not uniform due to the loss of continuity. At fully lithiated state (figure 2g), the estimated relative volume is 384%, close to the theoretical value 358%.[27] The delithiation process takes about 10 hours. SEM images were taken at the beginning and the end of the first plateau, at the end of the second plateau, and at the end of delithiation process, which are shown in Figures 2h – k. From points h to k, the relative volumes are 283%, 239%, 222% and 204%. At the beginning of the first plateau (point h), the relative volume has a large decrease from 384% to 283%. As the delithiation process is close to the end of the first plateau (point i), some concave areas appeared due to the large contraction of the material. At the end of the second plateau (point j), it is observed that some nanometer-sized pores start to appear mainly on the edge of the pulverized particle pieces. At the end of the delithiation process, the nanopores became larger, but the majority of the pores are on the edge of the pulverized particle pieces. As discussed in Ref [5, 13], the formation of pores is due to vacancy-mediated diffusion during the delithiation process. Our results show that the pores do not appear in the first plateau (transition from $Li_{22}Sn_5$ to LiSn). They start to form in the second plateau (transition from LiSn to $Li_2Sn_5$). The pores become larger in the third plateau probably due to the merging of pores, which is the transition from $Li_2Sn_5$ to Sn. It could be due to the large difference of Li diffusivity in Li-rich and

Li-poor phases. From points i to k, the relative volume has relatively small change from 239% to 204%. We believe that it is mainly due to the formation of pores. To verify that the formation of pores are not affected by the FIB polishing process, after the first cycle, we polished the particle from the other side. The morphology of the polished surface is shown in Figure S3. The FIB-SEM tomography was employed to reveal the porous structure in 3D as shown in Figure S4. The 3D image shows pores distributed across the particle. The larger pores are still mainly in the areas close to the edge of the pulverized particle pieces.

The same particle was transferred to a TEM grid after the above steps and a TEM specimen was prepared (Figure 3a). A JEOL JEM2100F TEM was employed for the microstructure analysis. Figure 3b is a low magnification micrograph of the area around a crack and a pore. Figures 3c and d are distribution of Sn and Li by energy-filtered TEM (EFTEM). The brighter means there is relatively more element. The result shows that Sn is uniformly distributed in the whole area. But Li is mainly distributed at the edge of the crack and the pore. Figure 3e is a high resolution TEM (HREM) image near the crack. There is a clear boundary between the crystal Sn and the amorphous $Li_xSn$. Figure 3f is the electron diffraction pattern of Sn which indicates the tin's crystal structure recovered after the delithiation process.

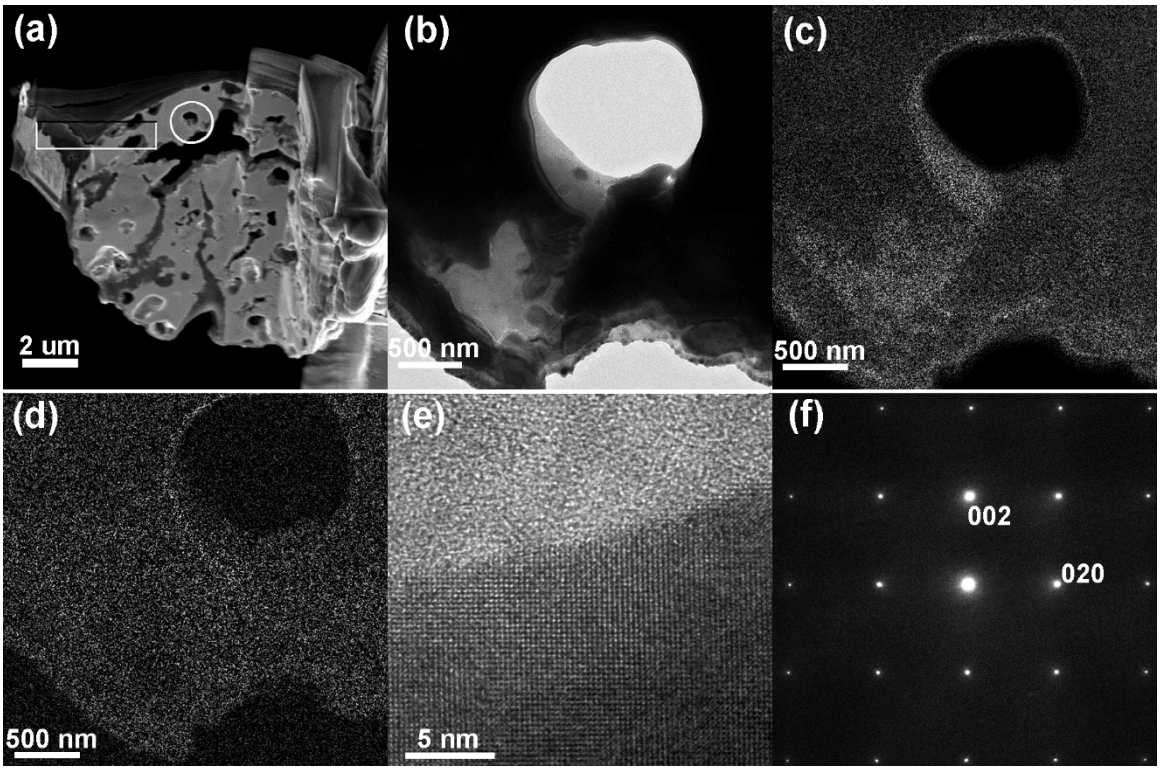


Figure 3. (a) SEM image of TEM sample after the final thin milling. (b) TEM image of the circled area in (a). (c) EFTEM mapping of Li. (d) EFTEM mapping of Sn. (e) HREM image near the crack. (f) Electron diffraction pattern of Sn.

In order to investigate the microstructural evolution under cycling and the potential capacity fading mechanisms, the same particle used to obtain the voltage profile shown in Figure S1a was cycled at 0.75 nA after the first cycle at 0.15 nA. As shown in Figure S5a, the capacity did not degrade after five cycles. It even increased a little in five cycles. It could be due to more complete lithiation of the Sn particle at high current when the surface area was increased during pulverization. However, Figures S5b and c show that the morphology of the particle is changed from a spherical shape with a smooth surface to an irregular shape with a rough surface. Figure S5d shows that the internal microstructure has become a completely porous structure. We can expect that the particle will pulverize completely and start to lose capacity when the cycling continues.

We also tested a Sn particle at higher current of 1.5 nA (about 3/5 C rate). The voltage profile, relative volume and SEM images at different states of charge are shown in Figure S6. The evolution of microstructure is similar to the particle tested at 0.3 nA. Cracks appear and increase during the lithiation process, porous structures are formed during the delithiation process. Due to the high current, the particle didn't reach its full discharge capacity. The relative volume is 255% at the end of lithiation process. We also can see that the third plateau in the delithiation process is very short. It means that the transition from $Li_2Sn_5$ to Sn is very short and most of the materials remain as $Li_2Sn_5$ or LiSn phases. As shown in Figure S6f, at the end of delithiation, the pores are not as large as the pores shown in Figures S3. It confirms that the merging of nanopores happens in the third plateau during the transition from $Li_2Sn_5$ to Sn.

It has been proposed that limiting the degree of Li uptake to the stoichiometry of LiSn relieves the pulverization problem to some extent. As shown in Figure 4, a Sn particle was tested with a limited discharge capacity of 0.9 nAh at 0.3 nA current. The particle was tested for two cycles. Figure 4a shows the voltage profile and relative volume. Figure 4b shows the particle in as-prepared condition. Figures 4c – f represent the same particle after the first discharging, the first charging, the second discharging and the second charging. Scanning ion beam images (Figures S7b-f) taken during cycling and SEM images (Figures S7g-h) taken from another angle after cycling illustrate the microstructural evolution. After the first discharging process, small cracks occur on the particle, but the polished surface is still intact. After the first charging, concave areas and pores start to appear on the polished surface. However, as shown in Figure 4a, only 38% of Li was removed from the particle and the

relative volume is decreased from 163% to 145%. It is probably due to the low Li diffusivity of Li-poor phases, which are the majority of Li-Sn alloy in this case. After the second discharging, the small cracks, which appeared during the first discharging propagate into the particle and more cracks are formed on the polished surface. After the second charging, porous structures are clearly shown on the particle. After the second cycle, the Li left in the particle in the first cycle is almost completely removed. We believe that it is due to the pulverization of the particle, which increases the active surface area and the inhomogeneity.

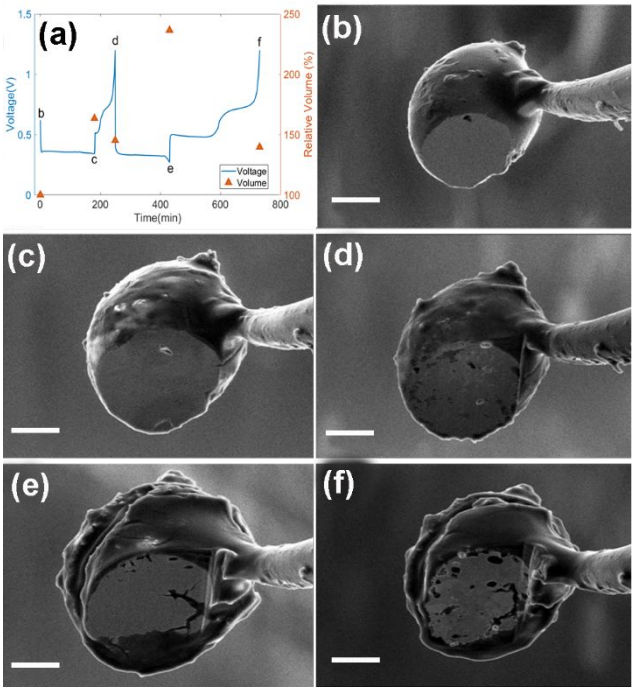


Figure 4. A Sn particle cycled with 0.9 nAh discharge limit and 0.3 nA current. a) Voltage profile and relative volume of the first two cycles. b-f) SEM images of the particle at the as-prepared, the first discharged, the first charged, the second discharged and the second charged states, respectively. Scale bar is 3 μm.

In summary, a single Sn particle battery cell has been built in the chamber of a FIB-SEM with vacuum environment by using ionic liquid electrolyte. This in situ cell provides a direct way to

measure and correlate the electrochemical performance and microstructural evolution of single Sn particle during cycling. Our results show the formation and evolution of cracks and porous structures at different states of charge during lithiation/delithiation processes. The electrochemical characteristics of the Sn particle are clearly affected by the microstructural evolution. This method is promising in the study of batteries to understand electrochemical reactions and mechanical degradation of high capacity battery materials.

**Acknowledgements**

This work was supported by the US National Science Foundation under Grant No. 1603847. This work was performed, in part, at the Center for Nanoscale Materials, an Office of Science user facility, was supported by the U.S. Department of Energy, Office of Science, Office of Basic Energy Sciences, under Contract No. DE-AC02-06CH11357.

**ASSOCIATED CONTENT**

Supporting Information available: [Comparison of the voltage profiles between a coin cell with Sn electrode and a single Sn particle cell, FIB images of a Sn particle fully discharged/charged at 0.3 nA, SEM image of the other side of a Sn particle fully discharged/charged at 0.3 nA, 3D reconstructed microstructure of the Sn particle shown in Figure 2, SEM images of a Sn particle after 6 cycles, SEM images of a Sn particle cycled at 1.5 nA, and FIB images of a Sn particle with limited discharge capacity.]

## References


1. Kamali, A.; Fray, D. J., *Tin-based materials as advanced anode materials for lithium ion batteries: A review*. 2011; Vol. 27.
2. Beaulieu, L.; Eberman, K.; Turner, R.; Krause, L.; Dahn, J., Colossal reversible volume changes in lithium alloys. *Electrochem. Solid-State Lett.* **2001,** *4* (9), A137-A140.
3. Zhang, M.; Wang, T.; Cao, G., Promises and challenges of tin-based compounds as anode materials for lithium-ion batteries. *Int. Mater. Rev.* **2015,** *60* (6), 330-352.
4. Dang, H. X.; Klavetter, K. C.; Meyerson, M. L.; Heller, A.; Mullins, C. B., Tin microparticles for a lithium ion battery anode with enhanced cycling stability and efficiency derived from Se-doping. *J. Mater. Chem. A* **2015,** *3* (25), 13500-13506.
5. Chao, S.-C.; Song, Y.-F.; Wang, C.-C.; Sheu, H.-S.; Wu, H.-C.; Wu, N.-L., Study on Microstructural Deformation of Working Sn and SnSb Anode Particles for Li-Ion Batteries by in Situ Transmission X-ray Microscopy. *The Journal of Physical Chemistry C* **2011,** *115* (44), 22040-22047.
6. Li, T.; Kang, H.; Zhou, X.; Lim, C.; Yan, B.; De Andrade, V.; De Carlo, F.; Zhu, L., Three-Dimensional Reconstruction and Analysis of All-Solid Li-Ion Battery Electrode Using Synchrotron Transmission X-ray Microscopy Tomography. *ACS Applied Materials & Interfaces* **2018,** *10* (20), 16927-16931.
7. Sun, F.; Markötter, H.; Zhou, D.; Alrwashdeh Saad Sabe, S.; Hilger, A.; Kardjilov, N.; Manke, I.; Banhart, J., In Situ Radiographic Investigation of (De)Lithiation Mechanisms in a Tin-Electrode Lithium-Ion Battery. *ChemSusChem* **2016,** *9* (9), 946-950.
8. Wang, J.; Chen-Wiegart Yu-chen, K.; Wang, J., In Situ Three-Dimensional Synchrotron X-Ray Nanotomography of the (De)lithiation Processes in Tin Anodes. *Angewandte Chemie International Edition* **2014,** *53* (17), 4460-4464.
9. Weker, J. N.; Liu, N.; Misra, S.; Andrews, J. C.; Cui, Y.; Toney, M. F., In situ nanotomography and operando transmission X-ray microscopy of micron-sized Ge particles. *Energy & Environmental Science* **2014,** *7* (8), 2771-2777.
10. Hua, L. X.; Yang, L.; Akihiro, K.; Sulin, Z.; Ting, Z.; Ju, L.; Yu, H. J., In Situ TEM Experiments of Electrochemical Lithiation and Delithiation of Individual Nanostructures. *Advanced Energy Materials* **2012,** *2* (7), 722-741.
11. Li, Q.; Wang, P.; Feng, Q.; Mao, M.; Liu, J.; Mao, S. X.; Wang, H., In Situ TEM on the Reversibility of Nanosized Sn Anodes during the Electrochemical Reaction. *Chemistry of Materials* **2014,** *26* (14), 4102-4108.
12. Liu, X. H.; Huang, J. Y., In situ TEM electrochemistry of anode materials in lithium ion batteries. *Energy & Environmental Science* **2011,** *4* (10), 3844-3860.
13. Wang, J.; Fan, F.; Liu, Y.; Jungjohann, K. L.; Lee, S. W.; Mao, S. X.; Liu, X.; Zhu, T., Structural Evolution and Pulverization of Tin Nanoparticles during Lithiation-Delithiation Cycling. *Journal of The Electrochemical Society* **2014,** *161* (11), F3019-F3024.
14. Cook, J. B.; Lin, T. C.; Detsi, E.; Weker, J. N.; Tolbert, S. H., Using X-ray Microscopy To Understand How Nanoporous Materials Can Be Used To Reduce the Large Volume Change in Alloy Anodes. *Nano Letters* **2017,** *17* (2), 870-877.
15. Huang, J. Y.; Zhong, L.; Wang, C. M.; Sullivan, J. P.; Xu, W.; Zhang, L. Q.; Mao, S. X.; Hudak, N. S.; Liu, X. H.; Subramanian, A.; Fan, H.; Qi, L.; Kushima, A.; Li, J., In Situ Observation of the Electrochemical Lithiation of a Single SnO<sub>2</sub> Nanowire Electrode. *Science* **2010,** *330* (6010), 1515.
16. Chen, C.-Y.; Sano, T.; Tsuda, T.; Ui, K.; Oshima, Y.; Yamagata, M.; Ishikawa, M.; Haruta, M.; Doi, T.; Inaba, M.; Kuwabata, S., In situ Scanning Electron Microscopy of Silicon Anode Reactions

in Lithium-Ion Batteries during Charge/Discharge Processes. *Scientific Reports* **2016,** *6*, 36153.
17. Marceau, H.; Kim, C.-S.; Paolella, A.; Ladouceur, S.; Lagacé, M.; Chaker, M.; Vijh, A.; Guerfi, A.; Julien, C. M.; Mauger, A.; Armand, M.; Hovington, P.; Zaghib, K., In operando scanning electron microscopy and ultraviolet–visible spectroscopy studies of lithium/sulfur cells using all solid-state polymer electrolyte. *Journal of Power Sources* **2016,** *319*, 247-254.
18. Miller, D. J.; Proff, C.; Wen, J. G.; Abraham, D. P.; Bareño, J., Observation of Microstructural Evolution in Li Battery Cathode Oxide Particles by In Situ Electron Microscopy. *Advanced Energy Materials* **2013,** *3* (8), 1098-1103.
19. Galiński, M.; Lewandowski, A.; Stępniak, I., Ionic liquids as electrolytes. *Electrochimica Acta* **2006,** *51* (26), 5567-5580.
20. Lewandowski, A.; Świderska-Mocek, A., Ionic liquids as electrolytes for Li-ion batteries—An overview of electrochemical studies. *Journal of Power Sources* **2009,** *194* (2), 601-609.
21. Yang, S.; Zavalij, P. Y.; Whittingham, M. S., Anodes for lithium batteries: tin revisited. *Electrochem. Commun.* **2003,** *5* (7), 587-590.
22. Cui, Y.; Li, T.; Zhou, X.; Mosey, A.; Guo, W.; Cheng, R.; Fu, Y.; Zhu, L., Electrochemical behavior of tin foil anode in half cell and full cell with sulfur cathode. *Electrochimica Acta* **2019,** *294*, 60-67.
23. Tamura, N.; Ohshita, R.; Fujimoto, M.; Fujitani, S.; Kamino, M.; Yonezu, I., Study on the anode behavior of Sn and Sn–Cu alloy thin-film electrodes. *J. Power Sources* **2002,** *107* (1), 48-55.
24. Winter, M.; Besenhard, J. O., Electrochemical lithiation of tin and tin-based intermetallics and composites. *Electrochim. Acta* **1999,** *45* (1-2), 31-50.
25. Wachtler, M.; Winter, M.; Besenhard, J. O., Anodic materials for rechargeable Li-batteries. *Journal of Power Sources* **2002,** *105* (2), 151-160.
26. Yang, J.; Takeda, Y.; Imanishi, N.; Yamamoto, O., Ultrafine Sn and SnSb0.14 Powders for Lithium Storage Matrices in Lithium-Ion Batteries. *Journal of The Electrochemical Society* **1999,** *146* (11), 4009-4013.
27. Ichitsubo, T.; Yukitani, S.; Hirai, K.; Yagi, S.; Uda, T.; Matsubara, E., Mechanical-energy influences to electrochemical phenomena in lithium-ion batteries. *Journal of Materials Chemistry* **2011,** *21* (8), 2701-2708.

**Table of Contents graphic**